Arab J Sci Eng (2016) 41:4397–4410
DOI 10.1007/s13369-016-2135-1

RESEARCH ARTICLE - MECHANICAL ENGINEERING

A Nonlinear Model for Incorporating the Coupled Effects of Surface Energy and Microstructure on the Electromechanical Stability of NEMS

Maryam Keivani[1] · Ali Koochi[2] · Hamid M. Sedighi[3] · Ahmadreza Abadian[4] · Mohamadreza Abadyan[2]

Received: 19 August 2015 / Accepted: 24 March 2016 / Published online: 16 April 2016

Abstract Surface energy and size phenomenon can play significant roles in physical performance of nano-electro-mechanical systems. Herein, the static and dynamic pull-in behavior of nano-tweezers and nano-switch fabricated from conductive cylindrical nano-wires is studied. The Gurtin–Murdoch surface elasticity in combination with the couple stress theory is employed to incorporate the coupled effects of surface energy and microstructure dependency (size phenomenon). Using Green–Lagrange strain, the higher-order surface stress components are incorporated in the nonlinear governing equation. The effect of gas damping is considered in the model as well as structural damping. The governing equation is solved using the reduced order method. The effects of various parameters on the static and dynamic pull-in parameters, phase plans and stability threshold of the nano-structures are demonstrated.

Keywords Couple stress theory · Surface effect · Cylindrical nano-wire · Dynamic pull-in instability

✉ Mohamadreza Abadyan
abadyan@yahoo.com

[1] Shahrekord University of Medical Sciences, Shahrekord, Iran

[2] Shahrekord Branch, Islamic Azad University, Sharekord, Iran

[3] Mechanical Engineering Department, Faculty of Engineering, Shahid Chamran University of Ahvaz, Ahvaz, Iran

[4] Mechanical Engineering Group, Kashan Branch, Islamic Azad University, Kashan, Iran

List of symbols

E	Young's modulus of the nano-wire
ν	Poisson ratio of the nano-wire
$\mu = E/2(1+\nu)$	Shear modulus of the nano-wire
l	Material length scale parameter
δ	Size effect non-dimensional parameter
E_0	Surface elastic modulus
e_0	Surface elastic modulus non-dimensional parameter
τ_0	Surface residual stress
t_0	Surface residual stress non-dimensional parameter
c_s	Structural damping coefficient
c_f	Gas damping coefficient
μ_f	Flow viscosity
$\gamma = 0.5572$	Euler's constant
K_n	Knudsen number
St	Stokes number
R	Radius of the nano-wire
L	Length of the nano-wire
D	Initial gap
f_{elec}	Electrical force
V	Applied voltage
$\varepsilon = 8.854 \times 10^{-12}$ $C^2\,N^{-1}\,m^{-2}$	Permittivity of vacuum
β	Applied voltage non-dimensional parameter
f_{vdW}	van der Waals force
$\bar{A} = (0.4-4) \times 10^{-19}$	Hamaker constant
η	Van der Waals force non-dimensional parameter
W	Nano-wire deflection
t	Time

1 Introduction

With recent advances in nano-fabrication, nano-wires have attracted many attentions in developing nano-electromechanical systems (NEMS). Nano-wire-fabricated nano-tweezers and nano-switches are of the most promising miniature systems that are promising for bio-engineering, medicine, electronics, nanoscale fabrications, sensing, mass-detecting, etc. A typical NEMS switch consists of a cantilever nano-wire suspended over a rigid conductive plane via a dielectric spacer in between. By applying DC potential difference, the nano-wire deflects toward the ground electrode until, at a critical voltage, it adheres the ground (pull-in). Typical NEMS tweezers are composed of two parallel nano-wire electrodes (arms) with a distance in between. By imposing electrostatic potential between the nano-wires, the wire tips move together and hence can manipulate ultra-small objects. It has been well recognized that determining the pull-in threshold is very crucial for designing credible switch and tweezers [1–6].

Nanoscale structural elements exhibit large surface area to volume ratio. Hence, the crucial influences of surface energy [7,8] on the behavior of the nano-structures might be considerable. While molecular dynamic simulation might be used for incorporating the surface layer in nano-elements, this approach is time-consuming and hence cannot easily be applied for modeling systems with large number of atoms. A continuum theory has been developed by Gurtin and Murdoch [9] to model the surface energy in miniature structures [7,8]. This theory is widely employed to simulate the impact of surface layer on mechanical behavior of nano-beams [10–12]. Recently, some researchers have studied the instability of NEMS incorporating the surface layer [12–17]. Fu and Zhang [12] have applied Gurtin–Murdoch elasticity to demonstrate the impact of surface energy on the stability of electromechanical bridges. Shaat and Mohamed [17] have investigated the static response of electromechanical microbeams incorporating the size phenomena and surface energy.

It has been well established that at the nanoscale separations (typically less than few nanometers) the presence of van der Waals (vdW) force substantially affects the pull-in instability of NEMS. Previous scientists have studied the effect of vdW force on adhesion and pull-in characteristics of ultra-small systems [4,18,19]. Wang et al. [19] investigated the effect of nanotube characteristics on the stability behavior under vdW force. The static instability of carbon nanotube nano-tweezers under the vdW attraction has been investigated in Refs. [20,21].

Beside the surface energy and vdW force, the effect of microstructure, i.e., size dependency of material characteristics at small scale, is another crucial issue that might be necessary to be considered in modeling NEMS. Experiments show a hardening trend in the elastic resistance of the materials such as conductive metals and nano-wires as the dimensions become comparable to the internal material length scale [22,23]. The classical continuum theory is not able to model the physical aspects of microstructure dependency of elastic constants at small scales. In this regards, the non-classical continuums such as non-local theory [24], couple stress theory (CST) [25], strain gradient [22] and modified couple stress elasticity [26] have been developed to investigate the size dependency of miniature structures. The CST can developed by imposing some restrictions on the micropolar theory which reduces the number of length scale parameters [27]. While other microstructure-dependent theories have been applied by many researchers to investigate miniature structures, less works have been conducted on modeling the ultra-small structures using the CST. Anthoine [28] studied bending of cylinders using the CST. The vibration of miniature beam based on the CST was studied in Ref. [29]. Fathalilou et al. employed the CST to investigate the microstructure-dependent bifurcation of an electromechanical system [30].

In the present study, the authors demonstrate the coupled influences of the microstructure and surface layer on the static and dynamic pull-in of NEMS fabricated from cylindrical nano-wire and operated in van der Waals regime. The CST in conjunction with Gurtin–Murdoch surface elasticity is applied to obtain the constitutive equations of cylinder–cylinder (for nano-tweezers) and cylinder–plate (for nano-switch) geometries. Using Green–Lagrange strain, the higher-order surface stress components are incorporated in the governing equation. NEMS structures are often subjected to the pressure of the gas flowed between the structure and the substrate. Hence, the gas flow damping is considered in the developed model. Analytical reduced order method (ROM) is applied to solve the governing equation.

2 Theoretical Model

Figure 1 depicts the schematics of ultra-small structures fabricated from nano-wire. Figure 1a presents typical nano-tweezers made of cantilever parallel conductive nano-wires. A typical NEMS switch fabricated form nano-wire is presented in Fig. 1b. The initial gap, length and the radius of the nano-wires are D, L and R, respectively.

2.1 Microstructure-Dependent CST

In the CST, the strain energy depends on the rotation gradient as well as the strain. The rotation tensor (ω) is explained as:

$$\omega_{ij} = \frac{1}{2}(u_{i,j} - u_{j,i}) = -\omega_{ji} \tag{1}$$

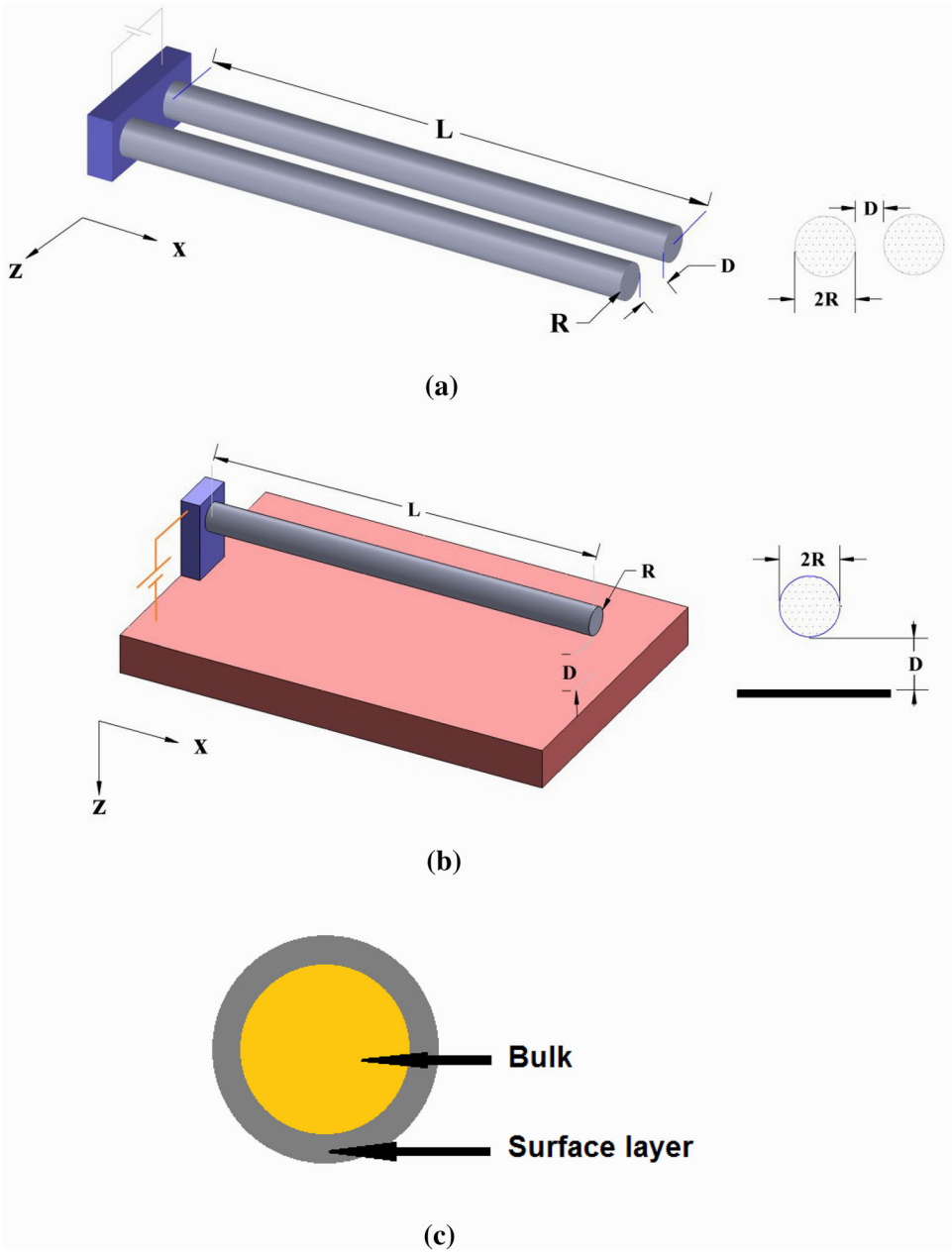

Fig. 1 **a** The schematic representation of nano-tweezers, **b** the schematic representation of nano-switch, **c** the schematics of the surface layer

The rotation vector (θ) is defined as:

$$\theta_i = \frac{1}{2} e_{ijk} u_{k,j} \tag{2}$$

where e_{ijk} is the permutation symbol. By eliminating the displacement u in Eqs. (1) and (2), we have:

$$\omega_{ij} = e_{ijk}\theta_k \tag{3a}$$

$$\theta_i = \frac{1}{2} e_{ijk}\omega_{jk} \tag{3b}$$

The gradient of rotation (κ) is defined as:

$$\kappa_{ij} = \theta_{j,i} = \frac{1}{2} e_{jkl}\omega_{kl,i} \tag{4}$$

Substituting Eq. (3) in Eq. (4), one can obtain:

$$\kappa_{ij} = \frac{1}{2} e_{jkl} u_{l,ki} \tag{5}$$

The bulk strain energy density ($\tilde{u}_B$) based on CST can be expressed as [29,32]:

$$\tilde{u}_B = \frac{1}{2}\lambda\varepsilon_{ij}\varepsilon_{ij} + \mu\varepsilon_{ij}\varepsilon_{ij} + 2\eta\kappa_{ij}\kappa_{ij} + 2\eta'\kappa_{ij}\kappa_{ij}, \tag{6}$$

where the nonlinear Green–Lagrangian strain tensor (ε_{ij}) is defined as follows:

$$\varepsilon_{ij} = \frac{1}{2}(u_{i,j} + u_{i,j} + u_{k,i}u_{k,j}), \tag{7}$$

In Eq. (6), λ and μ are Lame constants and shear modulus of the classical elasticity, whereas the moduli η and η' introduce the couple stress effects. Using Eq. (6), one can find the following relations:

$$\sigma_{ij} = \frac{\partial\tilde{u}}{\partial\varepsilon_{ij}} = \lambda\varepsilon_{mm}\delta_{ij} + 2\mu\varepsilon_{ij}, \tag{8a}$$

$$m_{ij} = \frac{\partial\tilde{u}}{\partial\kappa_{ij}} = 4\eta\kappa_{ij} + 4\eta'\kappa_{ji} \tag{8b}$$

where σ_{ij} is the classical stress tensor (symmetric) and m_{ij} is the couple stress tensor (deviatoric).

For an Euler beam, the displacement field is expressed as [33]

$$u_x(x, y, z, t) = -z\frac{\partial w(x,t)}{\partial x},$$
$$u_y(x, y, z, t) = 0, u_z(x, y, z, t) = w(x, t). \tag{9}$$

Using Eq. (9), one obtains:

$$\varepsilon_{xx} = -z\frac{\partial^2 w(x,t)}{\partial x^2} + \frac{1}{2}\left(z\frac{\partial^2 w(x,t)}{\partial x^2}\right) + \frac{1}{2}\left(\frac{\partial w(x,t)}{\partial x}\right)^2,$$

$$\varepsilon_{yy} = \varepsilon_{zz} = \varepsilon_{xy} = \varepsilon_{yz} = \varepsilon_{zx} = 0, \tag{10}$$

$$\sigma_{xx} = E\left(-z\frac{\partial^2 w\,(x,t)}{\partial x^2} + \frac{1}{2}z\frac{\partial^2 w(x,t)}{\partial x^2} + \frac{1}{2}\left(\frac{\partial w(x,t)}{\partial x}\right)^2\right),$$

$$\sigma_{yy} = \sigma_{zz} = \sigma_{xy} = \sigma_{yz} = \sigma_{zx} = 0, \tag{11}$$

$$\kappa_{xy} = -\frac{\partial^2 w(x,t)}{\partial x^2}, \quad \kappa_{xx} = \kappa_{yy} = \kappa_{zz} = \kappa_{yz} = \kappa_{zy} = \kappa_{zx} = \kappa_{xz} = \kappa_{yx} = 0 \tag{12}$$

$$m_{xy} = -4\eta\frac{\partial^2 w(x,t)}{\partial x^2}, \quad m_{yx} = -4\eta'\frac{\partial^2 W(x,t)}{\partial x^2},$$
$$m_{xx} = m_{yy} = m_{zz} = m_{yz} = m_{zy} = m_{zx} = m_{xz} = 0 \tag{13}$$

where E is the Young's modulus. Substituting Eqs. (10–13) in Eq. (6), the strain energy of bulk can be defined as:

$$U_B = \frac{1}{2}\int_0^L\int_A\left\{E\left[-z\frac{\partial^2 w}{\partial x^2} + \frac{1}{2}\left(-z\frac{\partial^2 w}{\partial x^2}\right)^2 + \frac{1}{2}\left(\frac{\partial w}{\partial x}\right)^2\right]^2 + 4\eta\left(\frac{\partial^2 w}{\partial x^2}\right)^2\right\}\mathrm{d}A\mathrm{d}x$$
$$= \frac{1}{2}\int_0^L\left\{(EI + 4\eta A)\left(\frac{\partial^2 w}{\partial x^2}\right)^2 + \frac{1}{4}EI^*\left(\frac{\partial^2 w}{\partial x^2}\right)^4 + \frac{1}{4}EA\left(\frac{\partial w}{\partial x}\right)^4 + \frac{1}{2}EI\left(\frac{\partial^2 w}{\partial x^2}\frac{\partial w}{\partial x}\right)^2\right\}\mathrm{d}x \tag{14}$$

In the above equation, A and I are area and moment of inertia of cross section, respectively. As shown, the strain energy does not depend on η' According to a previous investigation [32], the material constant η can be redefined as:

$$\eta = \mu l^2 \tag{15}$$

2.2 Strain Energy in the Surface Layer

According Gurtin–Murdoch elasticity [13], the in-plane components of the surface stress tensor are given by

$$\tau_{ij} = \mu_0\left(u_{i,j} + u_{j,i}\right) + (\lambda_0 + \tau_0)\,u_{k,k}\delta_{ij} + \tau_0\left(\delta_{ij} - u_{j,i}\right), \tag{16}$$

where μ_0 and λ_0 are the surface elastic constants, and τ_0 is the residual surface stress and the out-of-plane components of the surface stress tensor are given by [9]

$$\tau_{ni} = \tau_0\left(u_{n,i}\right). \tag{17}$$

By substituting relation (6) in Eqs. (16) and (17), one obtains

$$\tau_{xx} = \tau_0 + E_0\left(-Z\frac{\partial^2 w(x,t)}{\partial x^2} + \frac{1}{2}\left(-z\frac{\partial^2 w(x,t)}{\partial x^2}\right)^2 + \frac{1}{2}\left(\frac{\partial w(x,t)}{\partial x}\right)^2\right), \tag{18a}$$

$$\tau_{nx} = \tau_0\frac{\partial u_n(x, y, z)}{\partial x}, \tag{18b}$$

where $E_0 = \lambda + 2\mu_0$ is the surface elastic. The strain energy in the surface layer is written as

$$U_s = \frac{1}{2}\int_0^L\oint_{\partial A}(\tau_{ij}\varepsilon_{ij} + \tau_{ni}u_{n,i})\mathrm{d}s\mathrm{d}x \tag{19}$$

By substituting Eq. (8) and (17) in Eq. (18), the surface energy is determined as:

$$U_S = \frac{1}{2}\int_0^L \oint_{\partial A} \left\{ \begin{array}{l} \tau_0 \left(-z\frac{\partial^2 w}{\partial x^2} + \frac{1}{2}\left(-z\frac{\partial^2 w}{\partial x^2} \right)^2 + \frac{1}{2}\left(\frac{\partial w}{\partial x} \right)^2 \right) + \tau_0 n_Z^2 \left(\frac{\partial w}{\partial x} \right)^2 \\ + E_0 \left(-z\frac{\partial^2 w}{\partial x^2} + \frac{1}{2}\left(-z\frac{\partial^2 w}{\partial x^2} \right)^2 + \frac{1}{2}\left(\frac{\partial w}{\partial x} \right)^2 \right)^2 \end{array} \right\} \mathrm{d}s\mathrm{d}x$$

$$= \frac{1}{2}\int_0^L \left\{ \begin{array}{l} \frac{1}{2}\tau_0 C_0 \left(\frac{\partial w}{\partial x} \right)^2 + \frac{1}{2}\tau_0 I_0 \left(\frac{\partial^2 w}{\partial x^2} \right)^2 + \tau_0 S_0 \left(\frac{\partial w}{\partial x} \right)^2 + E_0 I_0 \left(\frac{\partial^2 w}{\partial x^2} \right)^2 + \frac{1}{4} E_0 I_0^* \left(\frac{\partial^2 w}{\partial x^2} \right)^4 \\ + \frac{1}{4} E_0 S_0 \left(\frac{\partial w}{\partial x} \right)^4 + \frac{1}{2} E_0 I_0 \left(\frac{\partial^2 w}{\partial x^2} \frac{\partial w}{\partial x} \right)^2 \end{array} \right\} \mathrm{d}x \tag{20}$$

where

$$I^* = \int_A z^4 \mathrm{d}A, \quad C_0 = \int_S \mathrm{d}s, \quad S_0 = \int_S n_z^2 \mathrm{d}s,$$
$$I_0 = \int_S z^2 \mathrm{d}s, \quad I_0^* = \int_S z^4 \mathrm{d}s \tag{21}$$

2.3 Work of External Force

Considering the distribution of $f_{\mathrm{ext}}(x,t)$, the work by the external forces is explained as:

$$W_{\mathrm{ext}} = \int_0^L \int_0^w f_{\mathrm{ext}}(x,t)\mathrm{d}w\mathrm{d}x. \tag{22}$$

In Eq. (22), the forces per unit length of the beam, $f_{\mathrm{ext}}(x,t)$, can be determined by the summation of vdW force with the electrostatic interaction.

2.3.1 Electrostatic Attraction

The nano-wires are considered as perfect cylindrical conductors. To determine the Coulomb force, the capacitance model is employed, which is described in two following sections.

Nano-switch

The nano-wire and plate are considered as perfect conductors. For a conductive cylinder with infinite length, the electrical energy per unit length is [34]

$$E_{\mathrm{elec}} = \frac{1}{2}C(D)V^2 = \frac{\pi\varepsilon_0 V^2}{\operatorname{arccosh}\left(1+\frac{D}{R}\right)} \tag{23}$$

where V and ε_0 are the applied voltage and the vacuum permittivity. Hence, the electrical attraction per unit length, f_{elec}, will be obtained by [35]

$$f_{\mathrm{elec}} = \frac{\mathrm{d}E_{\mathrm{elec}}}{\mathrm{d}D} = \frac{\pi\varepsilon_0 V^2}{\sqrt{D(D+2R)}\operatorname{arccosh}^2\left(1+\frac{D}{R}\right)} \tag{24}$$

Note that by applying DC voltage, the nano-wire deflects and the gap between the wire and the substrate reduces to $D-w$. Hence, by considering $D \pm R \approx D$, the electrical attraction per unit length of the deflected nano-wire is simplified as

$$f_{\mathrm{elec}} \approx \frac{\pi\varepsilon_0 V^2}{(D-w)\operatorname{arccosh}^2\left(\frac{D-w}{R}\right)} \approx \frac{\pi\varepsilon_0 V^2}{(D-w)\ln^2\left(2\frac{D-w}{R}\right)} \tag{25}$$

Nano-tweezers

The nano-wires are considered as perfect cylindrical conductors. Hence, the electrical energy per unit length that given by [34]

$$E_{\mathrm{elec}} = \frac{1}{2}C(D)V^2 = \frac{\pi\varepsilon_0 V^2}{\ln\left[1+\frac{D}{R}+\sqrt{\left(1+\frac{D}{R}\right)^2-1}\right]} \tag{26}$$

Hence, the electrostatic force per unit length is determined by [36]

$$f_{\mathrm{elec}} = \frac{\mathrm{d}E_{\mathrm{elec}}}{\mathrm{d}D} = \frac{\pi\varepsilon_0 V^2}{\sqrt{D(D+2R)}\ln^2\left(1+\frac{D}{R}+\frac{D}{R}\sqrt{1+\frac{2R}{D}}\right)} \tag{27}$$

In a similar deduction to NEMS, by applying the DC voltage on the nano-structure, the moveable arms will deflect to one another to reduce the gap from D to $D-w_1-w_2$. By assuming the identical geometry of the arms, the displacements of w_1, w_2 will be the same ($w_1 = w_2 = w$). Hence, by replacing D with $D-2w$ in relation (27) and considering that (R) is much less than the distance between the wires, we have:

$$f_{\mathrm{elec}} \approx \frac{\pi\varepsilon_0 V^2}{(D-2w)\ln^2\left(2\frac{D-2w}{R}\right)} \tag{28}$$

2.3.2 Intermolecular Attraction

A very simple model for describing the vdW force between bodies is the Lennard-Jones potential [37]. Ke and Espinosa

have presented a continuum model to evaluate the attractive intermolecular energy by volume integral of Lennard-Jones potential [38].

Nano-switch

For the nano-wire suspended over the half-space, by integrating over two volumes and assuming ($R < D$) the Lennard-Jones potential per unite length can be calculated as

$$E_{\text{vdw}} = -\frac{\pi^2 C_{1,2}\rho_1\rho_2 R}{3D^3} = -\frac{\bar{A}R^2}{3D^3} \tag{29}$$

where $\bar{A}$, which is in the range of $0.4{-}4 \times 10^{-19}$ J, is the Hamaker constant [39]. Now the vdW force per unit length, f_{vdW}, is determined as:

$$f_{\text{vdW}} = \frac{\mathrm{d}E_{\text{vdW}}}{\mathrm{d}D} = \frac{\bar{A}R^2}{D^4} \tag{30}$$

Note that by deflecting the nano-switch the initial gap between moveable nano-wire and fixed ground reduces from D to $D - w$, and therefore, the vdW force can be explained for deflected nano-wire as follows

$$f_{\text{vdW}} = \frac{\bar{A}R^2}{(D-w)^4}. \tag{31}$$

Nano-tweezers

For two nano-wires suspended over the space with the distance of D, by integrating over two volumes and assuming ($R < D$), the Lennard-Jones potential can be calculated as

$$E_{vdw} = -\frac{\bar{A}\sqrt{R}}{24D^{3/2}} \tag{32}$$

Now the intermolecular force per unit length, f_{vdW}, is determined as

$$f_{\text{vdW}} = \frac{\mathrm{d}E_{\text{vdW}}}{\mathrm{d}D} = \frac{\bar{A}\sqrt{R}}{16D^{5/2}} \tag{33}$$

By deflecting the nano-wires, their in-between distance reduces from g to $D - w_1 - w$. By assuming the identical geometry of the arms, the displacements of w_1, w_2 will be the same ($w_1 = w_2 = w$). Hence, the vdW attraction is obtained from Eq. (33) by replacing g with $D - 2w$

$$f_{\text{vdW}} = \frac{\bar{A}\sqrt{R}}{16(D-2w)^{5/2}} \tag{34}$$

2.4 Kinetic Energy and Damping Loss

The kinetic energy of nano-wire is determined as:

$$T = \frac{1}{2}\int_o^L \int_A \rho\left(\frac{\partial w(x,t}{\partial t}\right)^2 \mathrm{d}A\mathrm{d}x = \frac{1}{2}\int_0^L \rho\left(\frac{\partial w(x,t}{\partial t}\right)^2 \mathrm{d}x \tag{35}$$

And finally the virtual work W_d performed by damping effects can be expressed as:

$$W_d = \int_0^L \int_0^w (c_s + c_f)\frac{\partial w(x,t)}{\partial t}\mathrm{d}w\mathrm{d}x \tag{36}$$

where c_s is the structural damping coefficient and c_f is the gas damping coefficient that is obtained by calculating the drag force of a nano-wire and can be explained as [40].

$$c_s = \frac{4\pi\mu_f}{\log(4/St^*) - \gamma + 0.5 + cK_n} \tag{37a}$$

For systems operated at low Stokes numbers, the slip flow regime is dominant and

$$c_f = 4\pi\mu_f\left(\frac{St}{2}\right)^{\frac{1}{2}} \tag{37b}$$

For systems operated at high Stokes numbers, the no-slip flow regime should be considered. In the above equations, St is the Stokes number, μ_{f} is the flow viscosity, $St^* = \frac{R}{\upsilon}\frac{\partial w}{\partial t}$, $\gamma = 0.5572$ is Euler's constant, υ is the gas kinematic viscosity, $c \approx 1.8$ is a coefficient and K_n is the Knudsen number.

2.5 Hamilton Principle

The Hamilton principle is imposed to determine the constitutive equation of the structures,

$$\int_{t_1}^{t_2} (\delta T - \delta W_d - \delta U_B - \delta U_S + \delta W_{\text{ext}})\,\mathrm{d}t = 0 \tag{38}$$

Substituting Eqs. (14), (20), (22), (35) and (36) into (38) and some mathematical elaboration, one obtains:

$$\int_{t_1}^{t_2}\int_0^L \left[\begin{array}{l} \left(EI+4\mu Al^2+E_0I_0+\frac{1}{2}\tau_0I_0\right)\frac{\partial^4 w}{\partial x^4}-\left(\tau_0S_0+\frac{1}{2}\tau_0C_0\right)\frac{\partial^2 w}{\partial x^2}-\frac{3}{2}(EA+E_0C_0)\frac{\partial^2 w}{\partial x^2}\left(\frac{\partial w}{\partial x}\right)^2 \\ +\frac{3}{2}(EI^*+E_0I_0^*)\frac{\partial^4 w}{\partial x^4}\left(\frac{\partial^2 w}{\partial x^2}\right)^2+3(EI^*+E_0I_0^*)\frac{\partial^2 w}{\partial x^2}\left(\frac{\partial^3 w}{\partial x^3}\right)^2+\frac{1}{2}(EI+E_0I_0)\frac{\partial^4 w}{\partial x^4}\left(\frac{\partial^2 w}{\partial x^2}\right)^2 \\ +2(EI+E_0I_0)\frac{\partial w}{\partial x}\frac{\partial^2 w}{\partial x^2}\frac{\partial^3 w}{\partial x^3}+\frac{1}{2}(EI+E_0I_0)\left(\frac{\partial^2 w}{\partial x^2}\right)^3\rho A\frac{\partial^2 w}{\partial t^2}+(c_s+c_f)\frac{\partial w}{\partial t}-f_{\text{ext}}(x,t) \end{array}\right]\delta w\,\mathrm{d}x\,\mathrm{d}t$$

$$+\int_{t_1}^{t_2}\left[\begin{array}{l} \left(\tau_0S_0+\frac{1}{2}\tau_0C_0\right)\frac{\partial w}{\partial x}\delta w-\frac{1}{2}(EI+E_0I_0)\frac{\partial^3 w}{\partial x^3}\left(\frac{\partial w}{\partial x}\right)^2\delta w-\left(EI+4\mu Al^2+E_0I_0+\frac{1}{2}\tau_0I_0\right)\frac{\partial^3 w}{\partial x^3}\delta w \\ -\frac{1}{2}(EI+E_0I_0)\frac{\partial w}{\partial x}\left(\frac{\partial^2 w}{\partial x^2}\right)^2\delta w+\frac{1}{2}(EA+E_0C_0)\left(\frac{\partial w}{\partial x}\right)^3\delta w-\frac{3}{2}(EI^*+E_0I_0^*)\frac{\partial^3 w}{\partial x^3}\left(\frac{\partial^2 w}{\partial x^2}\right)^2\delta w \end{array}\right]_0^L \mathrm{d}t \tag{39}$$

$$+\int_{t_1}^{t_2}\left[\begin{array}{l} \frac{1}{2}(EI^*+E_0I_0^*)\left(\frac{\partial^2 w}{\partial x^2}\right)^3\delta\left(\frac{\partial w}{\partial x}\right)+(EI+E_0I_0)\frac{\partial^2 w}{\partial x^2}\left(\frac{\partial w}{\partial x}\right)^2\delta\left(\frac{\partial w}{\partial x}\right) \\ +\left(EI+4\mu Al^2+E_0I_0+\frac{\tau_0I_0}{2}\right)\frac{\partial^2 w}{\partial x^2}\delta\left(\frac{\partial w}{\partial x}\right) \end{array}\right]_0^L \mathrm{d}t+\int_0^L\left[\rho A\frac{\partial w}{\partial t}\delta w\right]_{t_1}^{t_2}\mathrm{d}X=0$$

The above equation reveals that each term must be zero. Therefore, by ignoring the higher-order terms the nonlinear governing equation of the system is obtained:

$$\begin{aligned} &\rho A\frac{\partial^2 w}{\partial t^2}+(c_s+c_f)\frac{\partial w}{\partial t} \\ &+\pi \mathrm{R}^2\left(\frac{1}{4}ER^2+4\mu l^2+E_0R+\frac{1}{2}\tau_0R\right)\frac{\partial^4 w}{\partial x^4} \\ &-\left(\tau_0S_0+\frac{1}{2}\tau_0C_0\right)\frac{\partial^2 w}{\partial x^2}=f_{\text{ext}}(x,t) \end{aligned} \tag{40}$$

and the boundary conditions are:

$$\begin{aligned} &\left(\tau_0S_0+\frac{1}{2}\tau_0C_0\right)\frac{\partial w}{\partial x} \\ &-\pi R^2\left(\frac{1}{4}ER^2+4\mu l^2+E_0R+\frac{1}{2}\tau_0R\right)\frac{\partial^3 w}{\partial x^3}\bigg|_{X=0,L}=0 \quad or \\ &\delta w|_{X=0,L}=0 \\ &\pi R^2\left(\frac{1}{4}ER^2+4\mu l^2+E_0R+\frac{1}{2}\tau_0R\right)\frac{\partial^2 w}{\partial x^2}\bigg|_{X=0,L}=0 \quad or \\ &\delta\left(\frac{\partial w}{\partial x}\right)\bigg|_{X=0,L}=0 \end{aligned} \tag{41}$$

2.6 Dimensionless Governing Equation

For cylindrical nano-wires with circular section, we have

$$I=\frac{\pi R^4}{4},\quad I_0=\pi R^3,\quad S_0=4\pi R,\quad C_0=2\pi R \tag{42}$$

Therefore, the governing equation of a nano-wire is obtained as:

$$\begin{aligned} &\rho\,\pi\,\mathrm{R}^2\frac{\partial^2 w}{\partial t^2}+(c_s+c_f)\frac{\partial w}{\partial t} \\ &+\pi\,\mathrm{R}^2\left(\frac{1}{4}\mathrm{R}^2E+4\mu l^2+\mathrm{R}E_0+\frac{1}{2}\mathrm{R}\tau_0\right)\frac{\partial^4 w}{\partial x^4} \\ &-5\,\pi\,\mathrm{R}\tau_0\frac{\partial^2 w}{\partial x^2}=f_{\text{elec}}(x,t)+f_{\text{vdW}}(x,t) \end{aligned} \tag{43a}$$

$$w(0)=\frac{\partial w}{\partial x}(0)=\frac{\partial^2 w}{\partial x^2}(\mathrm{L})=0 \tag{43b}$$

$$\begin{aligned} &5\pi R\tau_0\frac{\partial w}{\partial x}(L)-\pi R^2\left(\frac{1}{4}ER^2+4\mu l^2\right. \\ &\left.+E_0R+\frac{1}{2}\tau_0R\right)\frac{\partial^3 w}{\partial x^3}(L)=0 \end{aligned} \tag{43c}$$

The obtained governing equation and boundary conditions become dimensionless using relations (44):

$$X=\frac{x}{L}, \tag{44a}$$

$$W=\frac{w}{D}, \tag{44b}$$

$$k=\frac{D}{R}, \tag{44c}$$

$$\tau=\sqrt{\frac{E}{\rho}}\frac{R^2t}{2L^2} \tag{44d}$$

$$\delta=\frac{16\mu l^2}{R^2E} \tag{44e}$$

$$\xi=\frac{20\tau_0L^2}{R^3E} \tag{44f}$$

$$\beta^2 = \begin{cases} \frac{4\varepsilon_0 V^2 L^4}{ER^4 D^2} & \text{Nano-switch} \\ \frac{8\varepsilon_0 V^2 L^4}{ER^4 D^2} & \text{Nanotweezers} \end{cases}, \tag{44g}$$

$$\eta = \begin{cases} \frac{4\bar{A}L^4}{\pi R^2 E D^5} & \text{Nano-switch} \\ \frac{\bar{A}\sqrt{R}L^4}{2\pi R^4 E D^{7/2}} & \text{Nanotweezers} \end{cases}, \tag{44h}$$

$$\hat{c}_s = \frac{2c_d L^2}{\pi R^3 \sqrt{\rho E}} \tag{44i}$$

$$\hat{c}_f = \frac{2c_f L^2}{\pi R^3 \sqrt{\rho E}} \tag{44j}$$

$$e_0 = \frac{4E_0}{ER} \tag{44k}$$

Using (44), the general dimensionless equation is obtained as follows:

$$\frac{\partial^2 W}{\partial \tau^2} + (\hat{c}_s + \hat{c}_f)\frac{\partial W}{\partial \tau} + (1 + e_0 + \delta)\frac{\partial^4 W}{\partial x^4} - \xi \frac{\partial^2 W}{\partial x^2} = \begin{cases} \frac{\beta^2}{(1-W)\ln^2(2k(1-W))} + \frac{\eta}{(1-W)^4} & \text{Nano-switch} \\ \frac{\beta^2}{2(1-2W)\ln^2(2k(1-2W))} + \frac{\eta}{2(1-2W)^{5/2}} & \text{Nanotweezers} \end{cases} \tag{45a}$$

With the following B.C.:

$$W(0) = \frac{\partial W}{\partial x}(0) = 0 \tag{45b}$$

$$\frac{\partial^2 W}{\partial X^2}(1) = (1 + e_0 + \delta)\frac{\partial^3 W}{\partial X^3}(1) - \xi \frac{\partial W}{\partial X}(1) = 0 \tag{45c}$$

3 Solution

In order to solve Eq. (45), the displacement is expressed as a summation of independent functions $\varphi_i(x)$:

$$W(x) = \sum_{i=1}^{n} q_i \varphi_i(X) \tag{46a}$$

in the case of static problem and;

$$W(x, \tau) = \sum_{i=1}^{n} q_i(\tau)\varphi_i(X) \tag{46b}$$

in the case of dynamic problem, where the index i indicates the number of modes incorporated in the summation. The mode shapes of the nano-beam are selected as basic functions. The mode shapes of cantilever nano-beams can be expressed as:

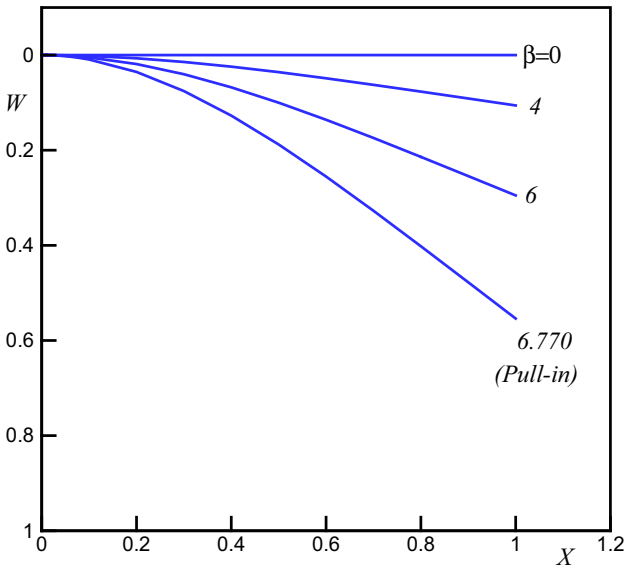

Fig. 2 Static deflections of the nano-switch for different values of β from zero to pull-in voltage

$$\varphi_i(X) = -\frac{\omega_i^2 \cos(\omega_i) + \lambda_i^2 \cos h(\lambda_i)}{\omega_i^2 \sin(\omega_i) + \lambda_i^2 \sin h(\lambda_i)} \times \left(\sin(\omega_i X) - \frac{\omega_i}{\lambda_i}\sin h(\lambda_i X)\right) + \cos(\omega_i X) - \cos h(\lambda_i X) \tag{47}$$

where ξ_i and λ_i are the ith roots of characteristic equation of cantilever beam which depends on the size and surface parameters.

By imposing Taylor expansion on force terms and substituting (46) in (45) afterward, following by multiplying the equation by $\varphi_i(x)$, and integrating from $X = 0$ to 1, the following system of algebraic equation is obtained:

$$(1 + \delta + e_0)\omega_i^4 q_i - \xi \int_0^1 \left(\varphi_i \sum_{j=1}^{N} q_j \frac{\mathrm{d}^2 \varphi_j}{\mathrm{d}X^2}\right) \mathrm{d}X - \int_0^1 \varphi_i \sum_{k=0}^{\infty} A_k \left(\sum_{j=1}^{N} q_j \varphi_j\right)^k \mathrm{d}X = 0, \quad \text{for } i = 1, 2, \ldots, N \tag{48a}$$

For static case and a system of ordinary differential equation for dynamic case as the following:

$$\int_0^1 \phi_i \phi_i \mathrm{d}x \ddot{q}_i + (\hat{c}_s + \hat{c}_f)\int_0^1 \phi_i \phi_i \mathrm{d}x \dot{q}_i + (1 + \delta + e_0) \int_0^1 \left(\phi_i \sum_{j=1}^{N} q_j \frac{\mathrm{d}^4 \phi_j}{\mathrm{d}x^4}\right) \mathrm{d}x$$

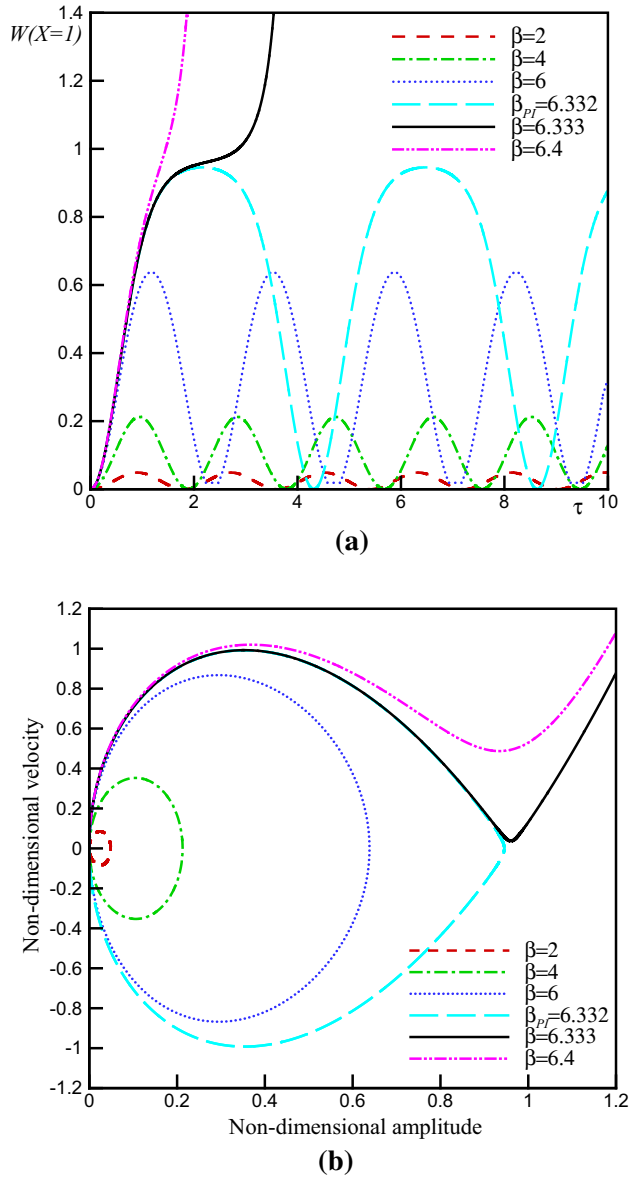

Fig. 3 Dynamic behavior of nano-switch by neglecting size, surface and damping effect for different values of β from zero to pull-in voltage, **a** time history, **b** phase plane

$$-\xi\int_0^1\left(\phi_i\sum_{j=1}^{N}q_j\frac{\mathrm{d}^2\phi_j}{\mathrm{d}x^2}\right)\mathrm{d}x-\int_0^1\phi_i\sum_{k=0}^{\infty}A_k\left(\sum_{j=1}^{N}q_j\phi_j\right)^k \mathrm{d}x=0,\quad for\ i=1,2,\ldots,N \tag{48b}$$

where N is the number of considered terms of ROM and A_k is defined as:

$$A_k=\begin{cases}\frac{\partial^k}{\partial W^k}\left[\frac{\beta^2}{(1-W)\ln^2(2k(1-W))}+\frac{\eta}{(1-W)^4}\right]\Big|_{W=0} & \text{Nano-switch}\\ \frac{\partial^k}{\partial W^k}\left[\frac{\beta^2}{2}(1-2W)\ln^2(2k(1-2W))+\frac{\eta}{2(1-2W)^{5/2}}\right]\Big|_{W=0} & \text{Nanotweezers}\end{cases} \tag{49}$$

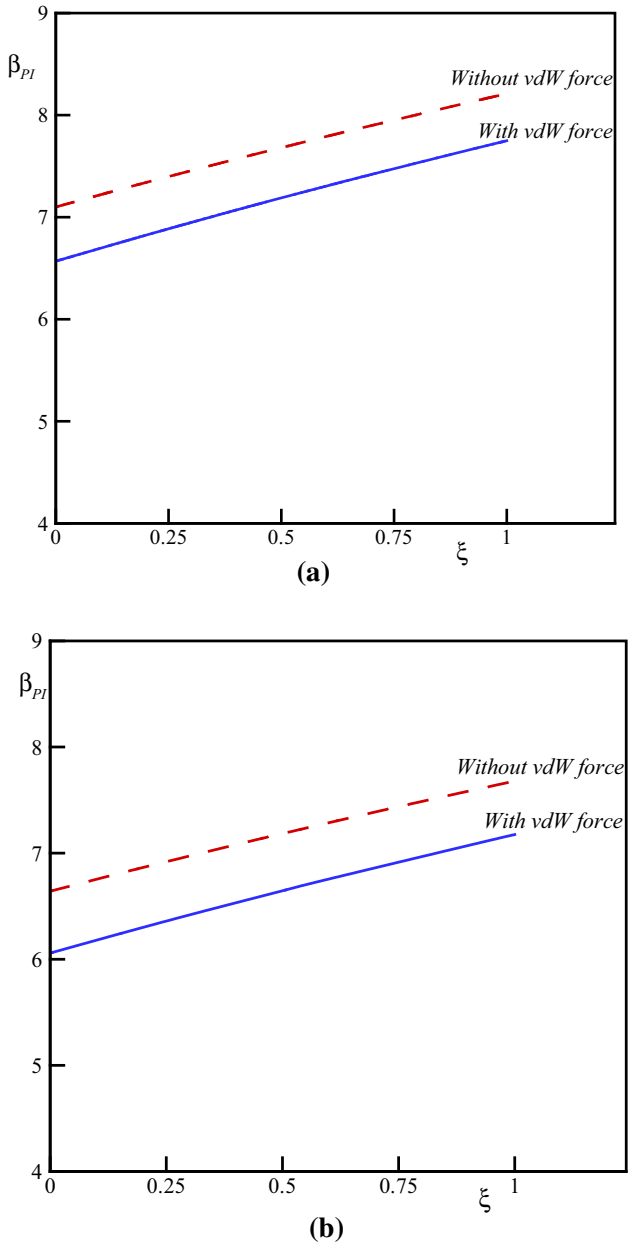

Fig. 4 Influence of surface energy on the pull-in voltage of nano-switch (neglecting size effects) $e_0=0.1$; $\eta=0.5$; $k=50$, **a** static, **b** dynamic

The algebraic system of equations (for static case) and system of ordinary differential equations (for dynamic case) are solved to determine the ROM solution. The instability parameters are determined via plotting the $W-\beta$ graphs.

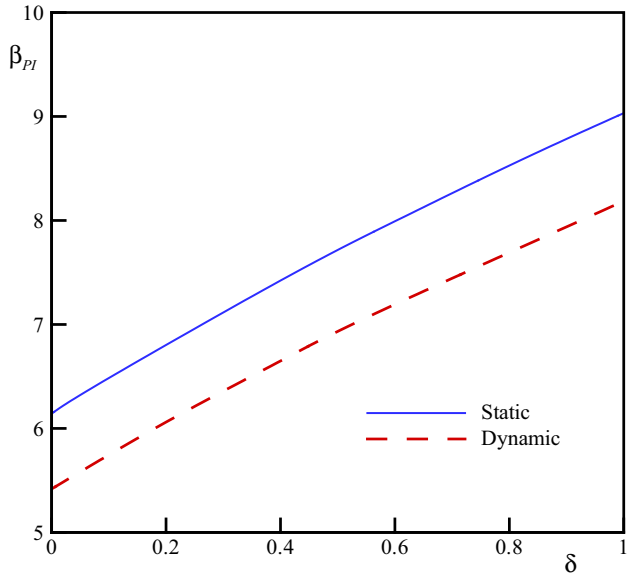

Fig. 5 Influence of size effect force on the pull-in voltage of nano-switch $e_0 = 0.1$; $\xi = 1$; $\eta = 0.5$; $k = 50$

4 Results

4.1 Nano-switch

Figure 2 depicts the variation of static defection of nano-switch when the voltage increases from zero to the instability values. In this figure, the microstructure and surface energy are neglected and the geometric parameter k is 50. This figure reveals that the static deflection of the switch increases by enhancing the applied voltage.

The time history and phase plane of the nano-switch for different voltages are shown in Fig. 3. This figure implies that maximum amplitude of the wire tip deflection increases by enhancing the DC voltage. If the DC voltage exceeds its critical value, β_{PI}, then the tip deflection increases rapidly and instability occurs. Figure 3 reveals that the phase plane has two fixed points; the stable center point and the unstable saddle node. The homoclinic orbit originates from the unstable branch saddle node and returns to it with the stable one. Beyond the unstable saddle node, the nano-beam collapses onto the substrate and becomes structurally unstable.

The impact of the surface energy on the instability threshold of nano-switch is presented in Fig. 4. This figure shows that by increasing the surface residual stress parameter ξ, the instability voltage enhances. Figure 4 reveals the surface stresses with the assigned parameters induce a hardening effect, i.e., increase the pull-in voltage. Furthermore, Fig. 4 shows that the presence of the vdW force decreases the pull-in voltage of nano-switch.

The influences of the microstructure-dependent size effect on the static and dynamic pull-in voltage of nano-switch are presented in Fig. 5. This figure reveals that an increase in the size parameter (δ) results in enhancing the instability voltage. Figure 5 demonstrates that the size effect induces a hardening effect in the pull-in behavior of the nano-wire-based switch. Furthermore, it is clear from this figure that the dynamic instability voltage of nano-wire is smaller than the static instability voltage as a result of inertia forces.

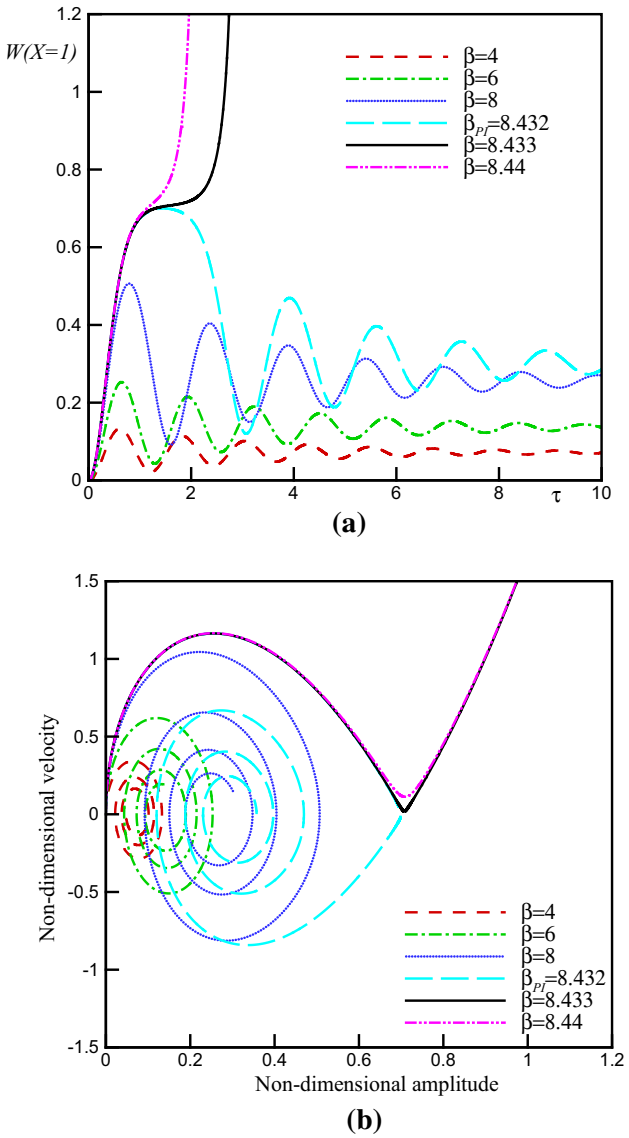

Fig. 6 Influence of damping parameter on the dynamic behavior of nano-switch $e_0 = 0.1$; $\xi = 1$; $\eta = 0.5$; $k = 50$; $\delta = 1$, **a** time history, **b** phase plane

The impact of the damping on the dynamic response of the nano-switch is illustrated in Fig. 6 for $\hat{c}_s = 0.3$; $\hat{c}_f = 0.3$. The obtained results show that the stable center equilibrium point becomes a stable focus point when the damping parameter is taken into account. It is concluded that the nano-wire exhibits convergent oscillations near the focus point in the presence of the damping and periodically oscillates in

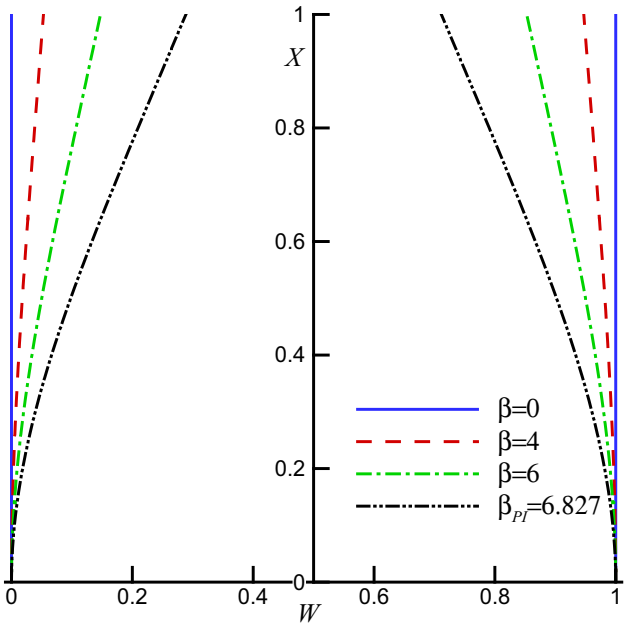

Fig. 7 Static deflections of the nano-tweezers for different values of β from zero to pull-in voltage

the absence of the damping. On the other hand, the second equilibrium point is unstable saddle point for any values of damping parameter. If the actuation voltage reaches the pull-in value, the trajectories which are attracted to the stable focus due to the damping effect diverge and the nano-structure becomes unstable.

4.2 Nano-tweezers

Figure 7 shows the variation of static defection of nano-tweezers when the voltage enhances from zero to the instability value. In this figure, the microstructure effect and surface layer are neglected and the geometric parameter k is 50. The figure implies that the static deflection of the nano-tweezers increases by increasing the applied voltage.

The time history and phase plane of the nano-tweezers for various voltage differences from zero to pull-in value is shown in Fig. 8. As seen, the maximum amplitude of wire tip increases by increasing the DC voltage. If the DC voltage exceeds its critical value, β_{PI}, then the tip deflection increases rapidly and instability occurs. Figure 8 reveals that the phase plane has two fixed points; the stable center point and the unstable saddle node. The homoclinic orbit originates from the unstable branch saddle node and returns to it with the stable one. Beyond the unstable saddle node, the nano-beam collapses onto the substrate and becomes structurally unstable.

The influences of surface energy on the pull-in threshold of the nano-tweezers are presented in Fig. 9. This figure shows that by increasing the surface residual stress parameter ξ, the pull-in voltage enhances. Figure 9 reveals that the surface stresses with the assigned parameters induce a hardening effect, i.e., increase the pull-in voltage. Furthermore, Fig. 9 shows that the vdW forces decrease the pull-in voltage of the nano-tweezers.

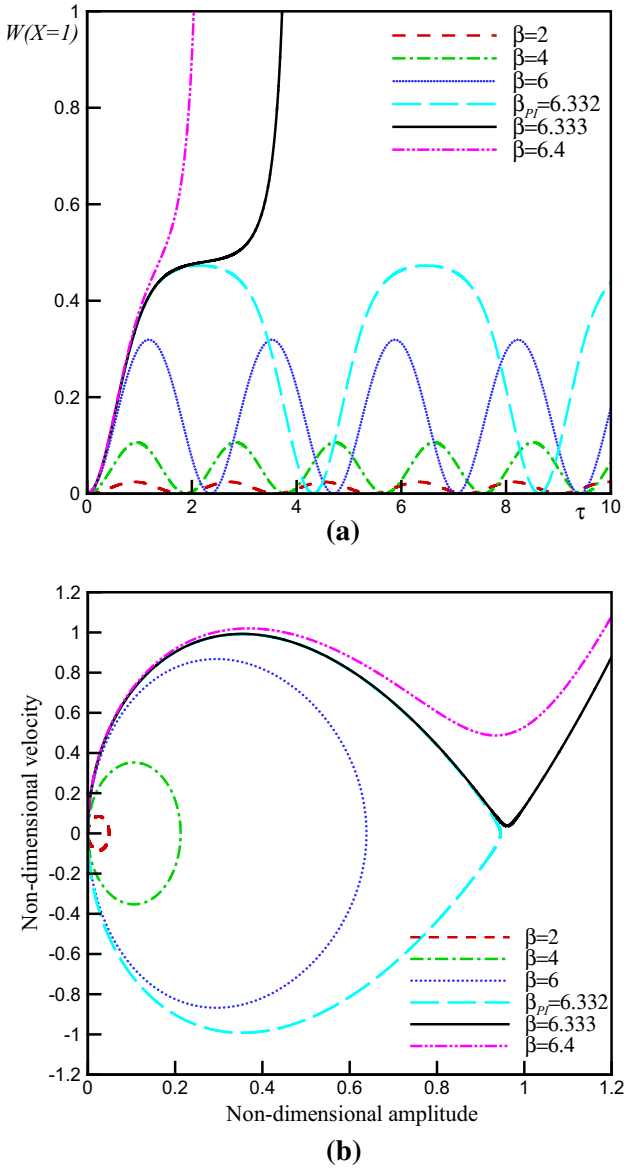

Fig. 8 Dynamic behavior of nano-tweezers by neglecting size, surface and damping effect for different values of β from zero to pull-in voltage, **a** time history, **b** phase plane

The influence of the size effect on the pull-in threshold of the nano-tweezers is shown in Fig. 10. This figure reveals that an increase in the size parameter (δ) results in elevating the instability voltage. Figure 10 demonstrates that the size effect induces a hardening effect in the pull-in behavior of the nano-wire-based tweezers. Furthermore, it is clear from this figure that the dynamic instability voltage of nano-wire is smaller than the static instability voltage as a result of the inertia.

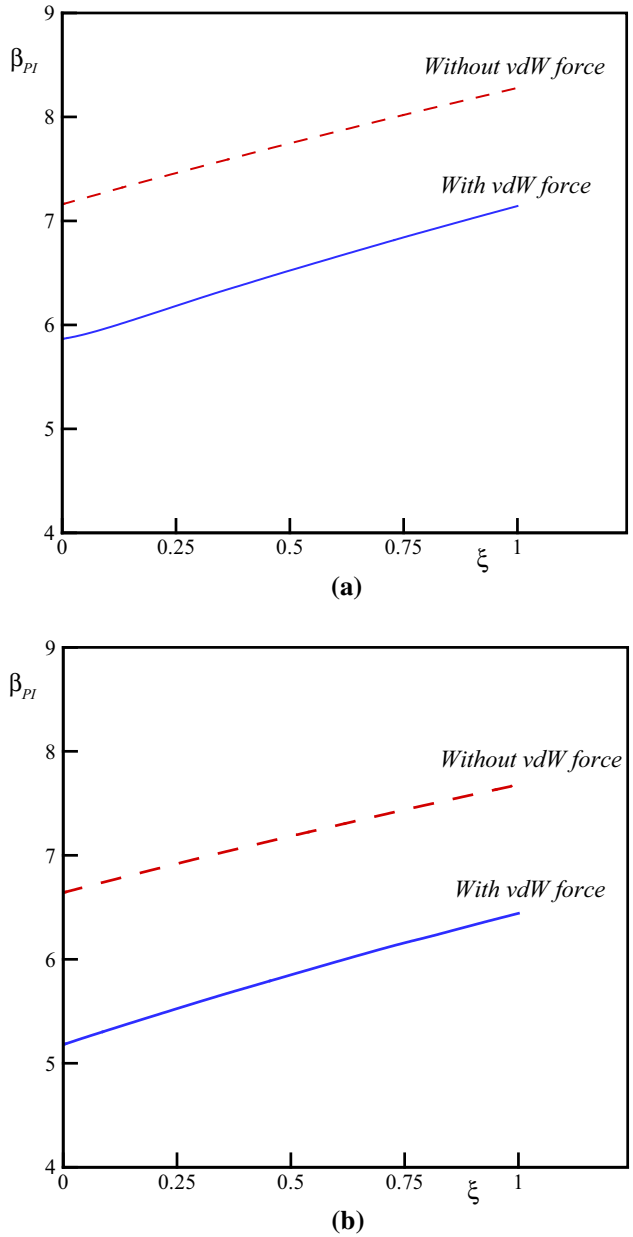

Fig. 9 Influence of surface energy on the pull-in voltage of nano-tweezers (neglecting size effects) $e_0 = 0.1$; $\eta = 0.5$; $k = 50$, **a** static, **b** dynamic

The influence of the damping on the dynamic behavior of vibrating nano-tweezers is illustrated in Fig. 11 for $\hat{c}_s = 0.3$; $\hat{c}_f = 0.3$. The obtained results show that the stable center equilibrium point becomes a stable focus point when the damping parameter is taken into account. It is found that the nano-tweezers exhibit convergent oscillations near the focus point in the presence of the flow damping and periodically oscillate in the absence of the damping. On the other hand, the second equilibrium point is unstable saddle point for any values of damping parameter. When the actuation voltage reaches the instability threshold, the trajectories

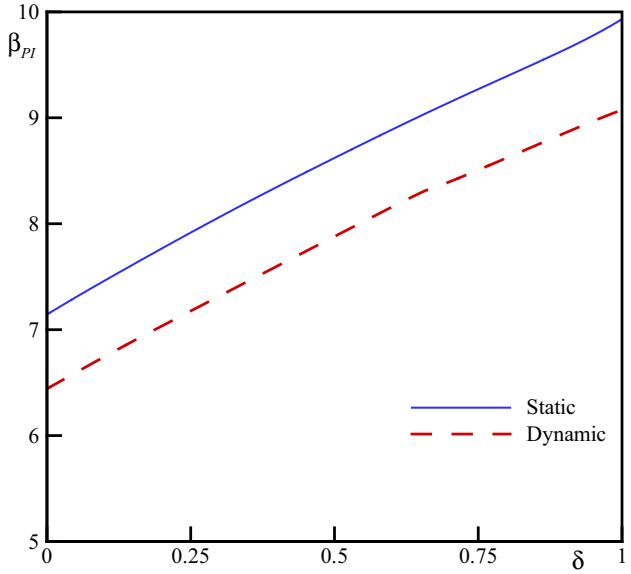

Fig. 10 Influence of size effect on the pull-in voltage of nano-tweezers $e_0 = 0.1$; $\xi = 1$; $\eta = 0.5$; $k = 50$

which are attracted to the stable focus due to the damping effect diverge and the nano-structure becomes unstable.

4.3 Validation

In order to validate the presented model, the nonlinear governing differential equation in the static case is solved, and the obtained results are compared with those of refs. [31,41]. In ref. [31], the instability voltage of carbon nano-wire nano-tweezers with a 6.9 μm initial gap, length of 19.6 μm and 150 nm wire radius was determined experimentally. Figure 12a depicts the SEM image of ultra-small tweezers fabricated from nano-wires. A chemical vapor deposition (CVD) system has been used for fabrication. In the fabrication process, the precursors ejected from the nozzles located next to the ion beam nozzle locally increase the pressure on a specific spot and chemically react with Ga+ ions such that physical deposition is gradually performed. The ion beam used for the nano-tweezers fabrication is 8.3 pA in current, 13 nm in diameter and 0.5 μm in dwell time. Phenanthrene vapor gas was used as deposition source material, and the length of the nano-wire is controlled by changing the dwell time and ion beam current in the fabrication machine. A spot beam irradiation has been used for the fabrication process. The tweezing motion was captured using an optical microscope with 1000× magnification. This case was also studied in ref. [41] numerically. As shown in Fig. 12b, the experimental measurements are slightly different from the ROM and numerical values were obtained by the classic continuum model. However, with the presented size-dependent model and considering the material length scale parameter $l = r/20$, one can find excellent consistency between them.

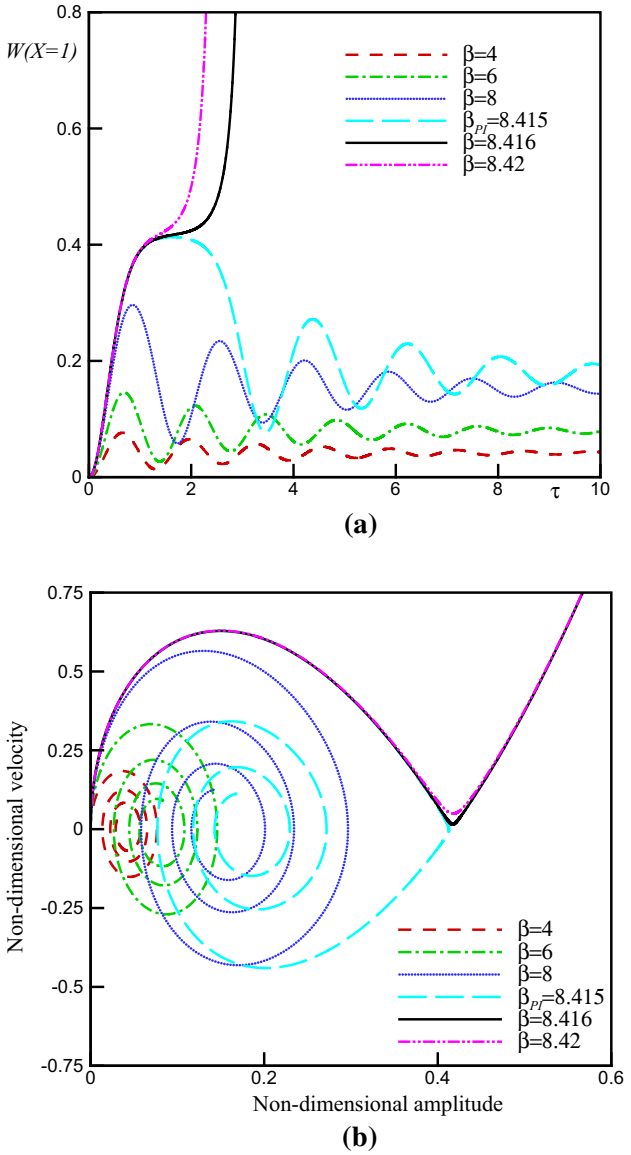

Fig. 11 Influence of damping parameter on the dynamic behavior of nano-tweezers $e_0 = 0.1; \xi = 1; \eta = 0.5; k = 50; \delta = 1$, **a** time history, **b** phase plane

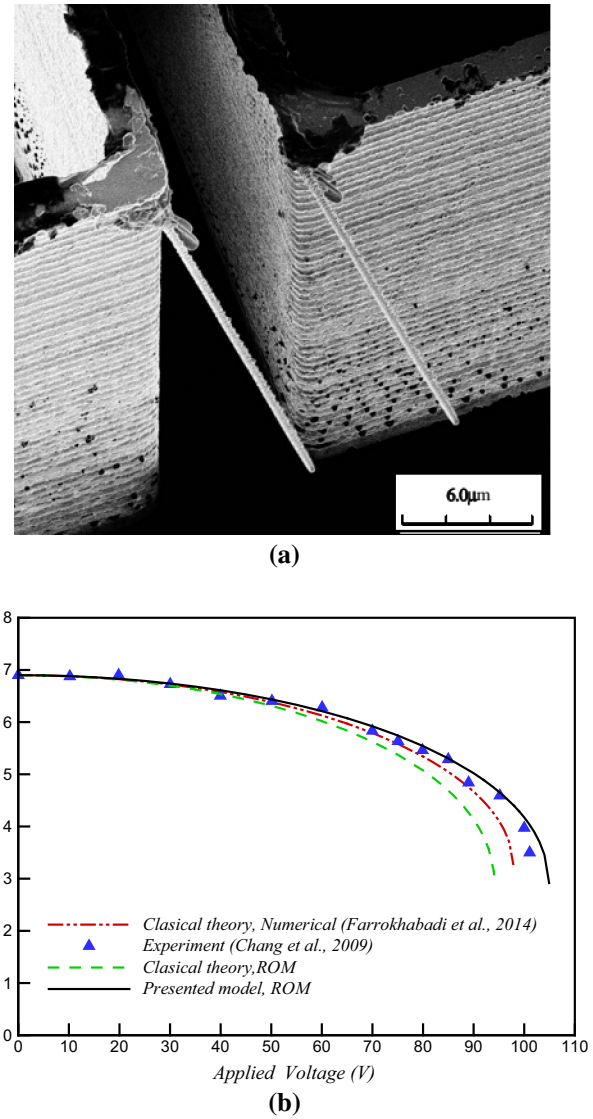

Fig. 12 **a** SEM image of nano-wire-based nano-tweezers [31], **b** comparison between the present model, experimental [31] and numerical results [41] for instability voltage

It confirms that the proposed approach is reliable for investigating device stability.

5 Conclusions

The influences of surface energy and microstructure on the static and dynamic pull-in threshold of the nano-wire-fabricated nano-switch and nano-tweezers were modeled incorporating the presence of vdW force and flow damping. The governing equation was solved using analytical reduced order method (ROM). The obtained results revealed that:

- The dynamic pull-in voltage of nano-beam is lower than static pull-in voltage as a result of the inertia.
- The surface layer with the assigned parameters induces a hardening effect, i.e., increases the pull-in voltage.
- The microstructure effect enhances the pull-in voltage of the nano-structures.
- The vdW force reduces the instability voltage of the nano-structures.
- When the gas damping effect is included in the simulations, the stable center point becomes the stable focus point.

References

1. Batra, R.C.; Porfiri, M.; Spinello, D.: Review of modeling electrostatically actuated microelectromechanical systems. Smart Mater. Struct. **16**(6), R23 (2007)

2. Batra, R.C.; Spinello, D.; Porfiri, M. : Pull-in instability in electrostatically actuated MEMS due to Coulomb and Casimir forces. In: Frangi, A.; Cercignani, C.; Mukherjee, S.; Aluru, N. (eds.) Advances in Multiphysics Simulation and Experimental Testing of MEMS, pp. 329–374. Imperial College Press, London (2007)
3. Batra, R.C.; Porfiri, M.; Spinello, D.: Effects of van der Waals force and thermal stresses on pull-in instability of clamped rectangular microplates. Sensors **8**(2), 1048–1069 (2008)
4. Abdi, J.; Koochi, A.; Kazemi, A.S.; Abadyan, M.: Modeling the effects of size dependence and dispersion forces on the pull-in instability of electrostatic cantilever NEMS using modified couple stress theory. Smart Mater. Struct. **20**(5), 055011 (2011)
5. Kooch, A.; Abadyan, M.: Efficiency of modified Adomian decomposition for simulating the instability of nano-electromechanical switches: comparison with the conventional decomposition method. Trends App. Sci. Res. **7**(1), 57–67 (2012)
6. Salekdeh, A.Y.; Koochi, A.; Beni, Y.T.; Abadyan, M.: Modeling effects of three nano-scale physical phenomena on instability voltage of multi-layer MEMS/NEMS: material size dependency, van der Waals force and non-classic support conditions. Trends App. Sci. Res. **7**(1), 1–17 (2012)
7. Gurtin, M.E.; Weissmüller, J.; Larche, F.: A general theory of curved deformable interfaces in solids at equilibrium. Philos. Mag. A **78**(5), 1093–1109 (1998)
8. Chen, T.; Chiu, M.S.; Weng, C.N.: Derivation of the generalized Young–Laplace equation of curved interfaces in nanoscaled solids. J. Appl. Phys. **100**(7), 074308 (2006)
9. Gurtin, M.E.; Murdoch, A.I.: A continuum theory of elastic material surfaces. Arch. Ration. Mech. Anal. **57**(4), 291–323 (1975)
10. He, J.; Lilley, C.M.: Surface effect on the elastic behavior of static bending nanowires. Nano Lett. **8**(7), 1798–1802 (2008)
11. Wang, G.F.; Feng, X.Q.: Surface effects on buckling of nanowires under uniaxial compression. Appl. Phys. Lett. **94**(14), 141913 (2009)
12. Fu, Y.; Zhang, J.: Size-dependent pull-in phenomena in electrically actuated nanobeams incorporating surface energies. Appl. Math. Model. **35**(2), 941–951 (2011)
13. Ma, J.B.; Jiang, L.; Asokanthan, S.F.: Influence of surface effects on the pull-in instability of NEMS electrostatic switches. Nanotechnolgy **21**(50), 505708 (2010)
14. Koochi, A.; Kazemi, A.; Khandani, F.; Abadyan, M.: Influence of surface effects on size-dependent instability of nano-actuators in the presence of quantum vacuum fluctuations. Physica Scripta **85**(3), 035804 (2012)
15. Wang, K.F.; Wang, B.L.: Influence of surface energy on the nonlinear pull-in instability of nano-switches. Int. J. Non Linear Mech. **59**, 69–75 (2014)
16. Ansari, R.; Mohammadi, V.; Shojaei M., F.; Gholami, R.; Darabi M., A.: A geometrically non-linear plate model including surface stress effect for the pull-in instability analysis of rectangular nanoplates under hydrostatic and electrostatic actuations. Int. J. Non Linear Mech. **67**, 16–26 (2014)
17. Shaat, M.; Mohamed, S.A.: Nonlinear-electrostatic analysis of micro-actuated beams based on couple stress and surface elasticity theories. Int. J. Mech. Sci. **84**, 208–217 (2014)
18. Soroush, R.; Koochi, A.; Kazemi, A.S.; Noghrehabadi, A.; Haddadpour, H.; Abadyan, M.: Investigating the effect of Casimir and van der Waals attractions on the electrostatic pull-in instability of nano-actuators. Phys. Scripta **82**(4), 045801 (2010)
19. Wang, G.W.; Zhang, Y.; Zhao, Y.P.; Yang, G.T.: Pull-in instability study of carbon nanotube tweezers under the influence of van der Waals forces. J. Micromech. Microeng. **14**(8), 1119 (2004)
20. Spengen, W.M.van ; Pures, R.; De Wolf, I.: A physical model to predict stiction in MEMS. J. Micromech. Microeng. **16**(1), 189 (2006)
21. Farrokhabadi, A.; Rach, R.; Abadyan, M.: Modeling the static response and pull-in instability of CNT nanotweezers under the Coulomb and van der Waals attractions. Phys. E **53**, 137–145 (2013)
22. Lam, D.C.C.; Yang, F.; Chong, A.C.M.; Wang, J.; Tong, P.: Experiments and theory in strain gradient elasticity. J. Mech. Phys. Solid **51**(8), 1477–1508 (2003)
23. McFarland, A.W.; Colton, J.S.: Role of material microstructure in plate stiffness with relevance to microcantilever sensors. J. Micromech. Microeng. **15**(5), 1060 (2005)
24. Eringen, A.C.; Edelen, D.G.B.: On nonlocal elasticity. Int. J. Eng. Sci. **10**(3), 233–248 (1972)
25. Ejike, U.B.: The plane circular crack problem in the linearized couple-stress theory. Int. J. Eng. Sci. **7**(9), 947–961 (1969)
26. Yang, F.A.C.M.; Chong, A.C.M.; Lam, D.C.C.; Tong, P.: Couple stress based strain gradient theory for elasticity. Int. J. Solid Struct. **39**(10), 2731–2743 (2002)
27. Asghari, M.; Kahrobaiyan, M.H.; Rahaeifard, M.; Ahmadian, M.T.: Investigation of the size effects in Timoshenko beams based on the couple stress theory. Arch. Appl. Mech. **81**(7), 863–874 (2011)
28. Anthoine, A.: Effect of couple-stresses on the elastic bending of beams. Int. J. Solid Struct. **37**(7), 1003–1018 (2000)
29. Fathalilou, M.; Sadeghi, M.; Rezazadeh, G.: Micro-inertia effects on the dynamic characteristics of micro-beams considering the couple stress theory. Mech. Res. Commun. **60**, 74–80 (2014)
30. Fathalilou, M.; Sadeghi, M.; Rezazadeh, G.: Gap dependent bifurcation behavior of a nano-beam subjected to a nonlinear electrostatic pressure. Lat. Am. J. Solid Struct. **11**(13), 2426–2443 (2014)
31. Chang, J.; Min, B.K.; Kim, J.; Lee, S.L.; Lin, L.: Electrostatically actuated carbon nanowire nanotweezers. Smart Mater. Struct. **18**, 065017 (2009)
32. Georgiadis, H.G.; Velgaki, E.G.: High-frequency Rayleigh waves in materials with micro-structure and couple-stress effects. Int. J. Solid Struct. **40**(10), 2501–2520 (2003)
33. Dym, C.L.; Shames, I.H.: Solid Mechanics. A Variational Approach. Railway Publishing House, Beijing (1984)
34. Li, M.; Bhiladvala, R.B.; Morrow, T.J.; Sioss, J.A.; Lew, K.K.; Redwing, J.M.; Keating, C.D.; Mayer, T.S.: Bottom-up assembly of large-area nanowire resonator arrays. Nat. Nanotechnol. **3**(2), 88–92 (2008)
35. Hayt, W.H.: Engineering Electromagnetics. McGraw-Hill Companies, (1981)
36. Farrokhabadi, A.; Rach, R.; Abadyan, M.: Modeling the static response and pull-in instability of CNT nanotweezers under the Coulomb and van der Waals attractions. Phys. E **53**, 137–145 (2013)
37. Lennard-Jones, J.E.: Perturbation problems in quantum mechanics. Proc. R. Soc. Lond. Ser. A **129**(811), 598–615 (1930)
38. Ke, C.H.; Espinosa, H.D.: Nanoelectromechanical systems (NEMS) and modeling. In: Handbook of Theoretical and Computational Nanotechnology, American Scientific Publishers, Valencia, CA (2006)
39. Guo, J.G.; Zhao, Y.P.: Dynamic stability of electrostatic torsional actuators with van der Waals effect. Int. J. Solid Struct. **43**(3), 675–685 (2006)
40. Berli, C.L.; Cardona, A.: On the calculation of viscous damping of microbeam resonators in air. J. Sound Vibr. **327**(1), 249–253 (2009)
41. Farrokhabadi, A.; Koochi, A.; Kazemi, A.; Abadyan, M.: Effects of size-dependent elasticity on stability of nanotweezers. App. Math. Mech. English Ed. **35**(12), 1573–1590 (2014)